Emission Lines in Active Galaxies: New Methods and Techniques
ASP Conference Series, Vol. 113, 1997
B.M. Peterson, F.-Z. Cheng, and A.S. Wilson (eds.)

Shocks and Photoionization in the Narrow-Line Region

Sueli M. Viegas

Instituto Astronômico e Geofísico, USP, São Paulo, Brazil

Marcella Contini

School of Physics and Astronomy, Tel-Aviv University, Ramat-Aviv, Tel-Aviv, Israel

Abstract. The presence of shocked regions in the narrow-line region (NLR) of active galactic nuclei (AGN) is discussed. Their effect on the physical conditions, in addition to photoionization from the central radiation source, is analyzed. We show that composite models, accounting for both shocks and photoionization, provide a consistent picture of the NLR which accounts for the observed emission-line and continuum spectra and is in agreement with the AGN unified model. The study of a particular object, NGC 5252, strengthens these results. It also shows that, besides explaining the observational data, the models make predictions that can be tested by infrared, optical, and X-ray imaging.

1. Introduction

Fifty years ago the emission-line spectra of the nuclei of galaxies observed by Seyfert (1943) showed similarities to those of planetary nebulae indicating that photoionization should be the main mechanism determining the physical conditions in the emission-line region. In five decades, the development of observational techniques helped draw a picture of these objects from the central engine to the extended emission-line region (EELR) which may extend to several hundreds of kpc. Several features and results inferred from observational data seem to indicate that an additional energy source is necessary, although its importance relative to the central radiation field may vary from one object to another.

The results from observations of the narrow-line regions (NLR) establish the basis for the models. The data come from many authors and we apologize for not including a comprehensive list of references. Recent observational data for the NLR can be found in several papers in this volume (the paper by Wilson, in particular). In the following, a summary of observed features and inferred results are given. We concentrate on those that help to determine the physical conditions in the NLR, its kinematics and the issues suggesting the presence of an energy source in addition to photoionization. Most of the results for the NLR and the EELR are similar. Therefore the EELR is explicitly referred to only when the data indicate different values.

1. As pointed out above, the similarities between the emission-line spectra of the NLR and of planetary nebulae indicate that photoionization must be powering the NLR (see, for instance, Osterbrock 1983). For the NLR, the presence of emission-lines from several ionization stages and the strength of low-ionization lines suggests that the relative number of high-energy to low-energy photons in the ionizing radiation field must be higher than in the usual black-body spectrum assumed for planetary nebulae, i.e., the AGN ionizing continuum must be flatter.

2. The optical continuum is usually fit by a power-law with a power-law index $-2 < \alpha < -1$ (Koski 1978, Osterbrock 1989, Malkan 1983). The ionizing continuum is then assumed to be an extrapolation of the optical continuum, and satisfies the condition stated above regarding its shape. The strength of the ionizing radiation field is usually characterized by the ionization parameter U, defined as the ratio between the density of ionizing photons and the gas density. Standard photoionization models assuming a power-law index of order -1.5 and $10^{-4} \leq U \leq 10^{-2}$ reproduce the main NLR spectral features.

3. *IRAS* data indicate that for most of the Seyfert 2 and narrow-line radio galaxies the far-infrared spectra are probably due to dust emission, while for LINERs the contribution from dust is not important and the spectra approach a power-law (Vaceli et al. 1993). Near-infrared observations of LINERs also indicate that dust emission is negligible (Willner et al. 1985).

4. The forbidden lines are density sensitive and set an upper limit to the electron density in the NLR (see, for instance, Osterbrock 1989). One of the strongest lines, [O III] λ5007, indicates that the density must be less than $10^7\,\mathrm{cm}^{-3}$. Another density indicator is the [S II] line ratio. Its values usually lead to densities in the range 10^3–$10^4\,\mathrm{cm}^{-3}$. For the EELR the [S II] line ratio gives an even lower density (Morganti et al. 1991, Prieto et al. 1993, Storchi-Bergmann et al. 1996).

5. The full width at half maximum (FWHM) of the emission lines is usually less than $2000\,\mathrm{km\,s}^{-1}$ (Osterbrock 1989), indicating that the NLR emitting clouds are moving slower than those in the BLR.

6. There is a correlation between the FWHM of a given emission line and its critical density, indicating that high-density clouds have higher velocities (Filippenko 1985).

7. The [O III] $\lambda5007/\lambda4363$ line ratio is a temperature indicator. For many objects this ratio is less than 100 (Contini & Aldrovandi 1986, Morganti et al. 1991), leading to high temperatures which cannot easily be reached in a photoionized gas. This may require an *additional heating process* for the emitting gas.

8. In order to explain the presence of such high-ionization lines as [S IV], [Si VII], [Fe VII] and [Fe X] in the observed spectra (Marconi et al. 1994, Oliva et al. 1994), the radiation field must be strong, i.e., the ionization parameter U must be higher than 10^{-1}. High U values imply that the

https://doi.org/10.1017/S0252921100040501 Published online by Cambridge University Press

photoionized gas has low density and is located closer to the center of the galaxy. Another possibility for explaining these high-ionization lines is to assume an *additional ionizing mechanism* for the NLR.

9. For an optically thick (radiation-bounded) cloud photoionized by a power-law continuum, the observed He II λ4686/Hβ ratio determines the spectral index of the ultraviolet spectrum. If the cloud is matter-bounded (i.e., the optical depth at the Lyman limit is close to unity), this ratio is not a good indicator of the ionizing radiation spectral shape, but it becomes an indicator of the optical depth. Several NLR and EELR seem to be matter bounded (Viegas-Aldrovandi 1988, Viegas & Prieto 1992, Binette et al. 1996).

10. The Hβ luminosity is proportional to the total number of ionizing photons absorbed by the gas. Usually a power-law spectrum characterized by the parameters given in (2) gives an Hβ luminosity lower than observed. If the NLR is not optically thick, the problem of the missing photons is even worse. This may be another indication that an *additional ionizing mechanism* is operating in the NLR.

In the past two types of additional ionization mechanisms for the NLR have been invoked: high-energy particles (Ferland & Mushotzky 1984, Viegas-Aldrovandi & Gruenwald 1988, 1990), and shocks (Contini & Aldrovandi 1983, Binette et al. 1985). The cloud velocities, the correlation between the velocity and the density, the detection of jets associated with emission lines, and the recent *HST* images of shock fronts in the Seyfert NLR (Pogge, this volume) seem to indicate that shocks are playing a role in the NLR. The results of models where both photoionization and shocks are powering the NLR are discussed in the following sections.

2. Steady-State Shocks and Photoionization

About 25 years ago, a steady-state shock model was built to explain the observed spectrum of the Cygnus Loop (Cox 1972). At that time, the prediction that the Balmer lines would be enhanced by collisions, and the Balmer decrement due to shock waves should then be steeper than that due to radiative recombination, was not confirmed by the observations. Cox's model showed that the very high-temperature gas in the post-shock zone produces ultraviolet photons which ionize the gas in the cooler regions, while if the cooling is fast and the temperature drops before the ions recombine, the collisional excitation is not efficient, and the Balmer decrement should approach the radiative value as proposed by Parker (1967) and Poveda & Woltjer (1968). In fact, in a heated gas free-free and free-bound collisions produce an ultraviolet radiation field (the so-called diffuse or secondary radiation in photoionization models) which efficiently heats and ionizes the gas in the low-temperature zone. The presence of this diffuse radiation, creating an H II region farther from the shock front, led Dopita and collaborators to call their shock models 'autoionizing shock models' (Sutherland, Bicknell, & Dopita 1993). However, this is misleading since 'autoionization' is a well-known atomic-physics process and has nothing to do with the diffuse radiation field.

https://doi.org/10.1017/S0252921100040501 Published online by Cambridge University Press

As the supersonic material goes through the shock front, the particle's ordered velocity is diverted and thermalized, the velocity of the flow drops and, because of the continuity of the mass flow, the density increases. This is equivalent to a traffic jam. If the cooling length in the high-temperature zone is much smaller than the radius of curvature of the filament (or cloud) and the crossing time of the cooling region is smaller than the temporal variation of the shock velocity, the problem can be treated as a steady-state plane-parallel flow. The fluid equations are given by Cox (1972) and include the continuity of the mass flow, pressure equilibrium across the shock front and the energy equation. The effect of magnetic pressure is to reduce the gas compression. If a frozen-in magnetic field is present, the maximum compression is given by $(n/n_0)^2 = 8\pi P_0/B_0$ where n_0, P_0, and B_0 are respectively the preshock number density, the pressure, and the magnetic-field component perpendicular to the shock velocity. The calculations should follow a parcel of gas in the matter flow. However, in a steady-state, the temporally integrated spectrum of a given parcel is the same as the spatially integrated spectrum of all the parcels with different ages (defined as the time since a parcel crossed the shock front). For this case, the temperature and density distribution in a shocked region is illustrated in Fig. 1 (top panel). The cooling zone, the recombination zone, and the H II region due to the diffuse radiation originating in the hot gas are labeled C, R and DR respectively . The electron density is indicated by a dashed line.

For many years different authors used shock-model results for supernova remnants in diagnostic diagrams for the NLR. However, if shocks are present in the NLR, the velocities indicated by the FWHM are higher than those found in SNR. Since the temperature in the cooling zone is $T \approx 10^6 (v_s/300\,\mathrm{km\,s^{-1}})^2\,\mathrm{K}$, higher-velocity shocks have a higher-temperature post-shocked zone, a different cooling rate, and a stronger diffuse radiation field leading to different physical conditions and different line intensities. Therefore SNR models are not appropriate to fit the NLR observed spectrum. In addition, *it is not possible to turn off the central engine and forget about the effect of the central radiation in a shocked region.* More realistic models for the NLR must take into account photoionization by the central radiation field.

A series of composite models incorporating for both shock and photoionization effects have been built for the NLR assuming shock velocities $v_s \geq 100\,\mathrm{km\,s^{-1}}$, a power-law spectrum with index $\alpha = -1.5$ for the central radiation field with different intensities of the radiation flux at the Lyman limit (F_H), and assuming a cosmic abundance for the gas. The photons from the central source may reach the cloud on the same side or on the opposite side of the shock front. The schematic distribution of temperature and density in this latter case is illustrated in Fig. 1b where PR indicates the zone photoionized by the primary (central) radiation and TZ is the transition zone, which is photoionized by the the diffuse radiation coming from both sides of the cloud. The width of this zone depends on the strength of the diffuse radiation field and on the physical width of the cloud. Details on the calculations, physical processes, and atomic data are given in Viegas & Contini (1994) and references therein.

The models for the NLR are built using the code SUMA, which in its latest version (Viegas & Contini 1994) solves the equations taking into account 12 elements (H, He, C, N, O, Ne, Mg, Si, S, Cl, A, and Fe) and the effect of dust. The input parameters are the chemical abundances (usually from Allen 1973),

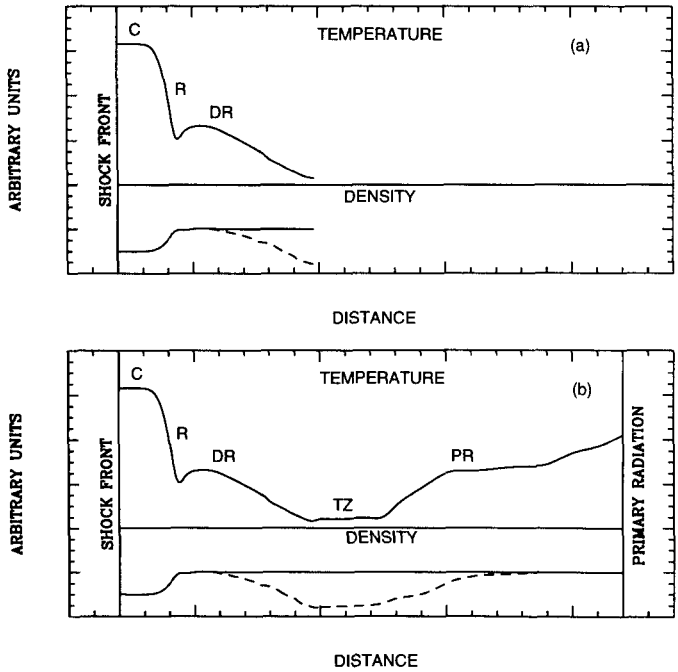

Figure 1. Temperature and density distributions: (a) steady-state plane-parallel shock — C, R and DR indicate the cooling region, the recombination region, and the zone ionized by the diffuse radiation, respectively; (b) shock-photoionization composite model — TZ indicates the transition zone, and PR the region photoionized by the primary radiation originating in the central source. The dashed line corresponds to the electron density.

https://doi.org/10.1017/S0252921100040501 Published online by Cambridge University Press

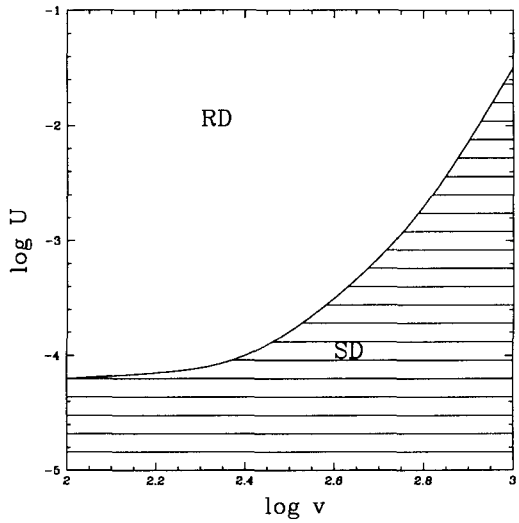

Figure 2. Shock-dominated (SD) and radiation-dominated (RD) models.

the dust-to-gas number ratio, the shock velocity v_s, the preshock density n_0, the magnetic field B_0, and the ionizing-radiation spectrum characterized by the flux intensity at the Lyman limit and its shape (usually a power-law is adopted with index $\alpha = -1.5$).

A first test of our models was the comparison of the the emission-line results with observational data for several AGN using the diagnostic diagrams and fitting the infrared and optical continua. Once the main trends concerning the best way to fit the data were established, the next step was to fit the continuum and the emission-line spectra of a given object for which data in a larger range of wavelength (far infrared to X-rays) are available. These results are discussed in the next section.

3. A Consistent Scenario for the NLR

3.1. General Model Results

Depending on the shock velocity and on the strength of the central ionizing radiation, the physical conditions in the cloud and, consequently, the emission-line luminosities are dominated either by the shock effect or by the primary-radiation photoionization. Measuring the ionization parameter U at the edge of the cloud reached by the primary photons and characterizing the shock strength by its velocity v_s, Fig. 2 shows the values of U and v_s for which the cloud is shock-dominated (SD) or radiation-dominated (RD). The limit between the two regions corresponds to the values where the Hβ intensity due to shocks is equal to that due to photoionization by the central source. Notice that:

https://doi.org/10.1017/S0252921100040501 Published online by Cambridge University Press

- the intensity due to the shock already includes the contribution from the diffuse radiation originating in the cooling zone;
- we have assumed that the area reached by the central photons is equal to the shocked area, since it is the same plane-parallel cloud;
- high-luminosity AGN (i.e, high NLR ionization parameter) have predominantly RD clouds unless the velocity is greater than $40\,\mathrm{km\,s^{-1}}$, whereas low-luminosity AGN may have SD clouds at lower velocities.

In addition, from grids of models built to fit the observational data of a large sample of NLR of different types of AGN (Viegas & Contini 1994 and references therein), some other general results emerge:

- The RD models show emission-line intensities normally obtained from standard photoionization models. Thus, with cosmic abundances the temperature of the gas is smaller than $2 \times 10^4\,\mathrm{K}$, which cannot account for some of the observed [O III] line ratios. Moreover, the continuum radiation emitted by these clouds is in the infrared-optical range.
- Shocks with $v_s \geq 300\,\mathrm{km\,s^{-1}}$ lead to a high-temperature zone which produces ultraviolet and soft X-ray continuum emission and high-ionization emission-lines such as [Fe X]. In addition, this high temperature-zone helps to solve the problem of the observed low values for the [O III] $\lambda 5007/\lambda 4363$ line ratio.
- The magnetic field intensity determines the compression of the gas. From previous fits to NLR spectra (Contini & Aldrovandi 1986), a value $B_0 \approx 10^{-4}$ Gauss seems adequate.
- The dust-to-gas ratio and the shock velocity determine if the far-infrared emission is due to dust or not. Adopting a silicate grain size of $0.2\ \mu$, the dust temperature in the PR zone (Fig. 1b) is always lower than 100 K whereas in the C zone it may reach a higher temperature. Grain survival against sputtering in the shocked zone decreases with increasing v_s, and for $v_s \geq 300\,\mathrm{km\,s^{-1}}$, the width of the survival zone is $\leq 3 \times 10^{15}\,\mathrm{cm}$.

3.2. Parameters for the NLR

First let us notice that if shocks are present in the NLR: (a) it is easily understood from shock compression that high-velocity clouds are high-density clouds as is inferred from the correlation between the FWHM and the critical density of the forbidden lines; (b) shocks provide the *additional energy source* required by the high temperature indicated by the [O III] line ratio in several objects, the presence of high-ionization lines, and by the missing ionizing photons; (c) shocks can heat dust present in the cloud in order to reproduce the far-infrared emission; and (d) high-velocity shocks may explain the soft X-ray continuum observed in AGN.

It is expected that both RD and SD clouds with different velocities and dust-to-gas ratios are present in NLR of the various types of AGN. Thus, the fitting of the observed emission-line ratios using the diagnostic diagrams and

https://doi.org/10.1017/S0252921100040501 Published online by Cambridge University Press

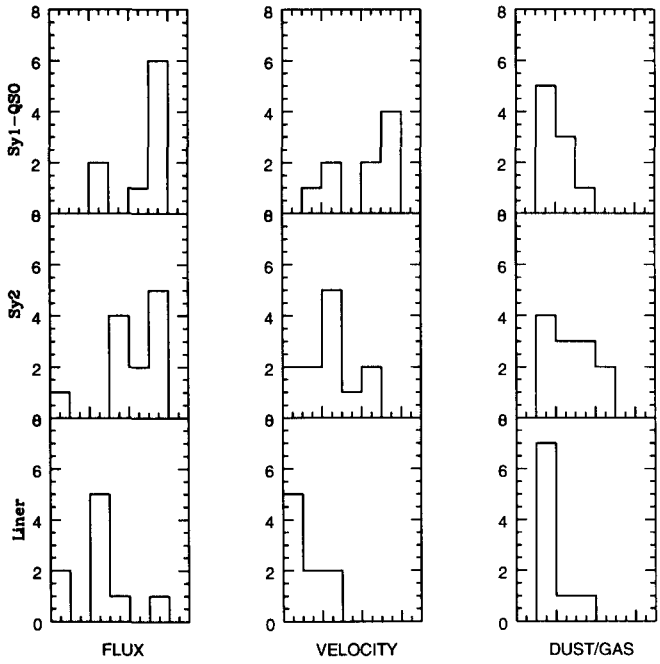

Figure 3. Parameters for the NLR of AGN. The bin ranges are $7 \leq \log F_{\rm H} \leq 13$ for the ionizing flux, $100 \leq v_s \leq 700\,{\rm km\,s^{-1}}$ for the shock velocity, and $-15.5 \leq \log(d/g) \leq -12.5$ for the dust-to-gas ratio.

of the infrared-optical continua gives only the characteristic parameters of the dominant type of cloud producing the observed spectra. From the diagnostic diagrams, we obtain the range of variation of the main input parameters: $100 \leq v_s \leq 600\,{\rm km\,s^{-1}}$, $10^7 \leq F_{\rm H} \leq 10^{12}\,{\rm cm^{-2}\,s^{-1}\,eV^{-1}}$. In addition, fitting the infrared-optical continua indicates a dust-to-gas number ratio in the range $10^{-14} \leq d/g < 10^{-12}$.

The results for a sample of QSOs, Seyfert 1 and 2 galaxies, and LINERs are summarized in Fig. 3. Keeping in mind the observational results listed in §1, this figure shows that our composite models provide a coherent scenario for the NLR which is consistent with the observations and with the unified model for AGN, as discussed briefly below.

The intensity of the ionizing radiation seems to be stronger for QSOs and Seyfert 1 galaxies than for Seyfert 2 galaxies, which is expected if the so-called unified model for AGN applies (see other papers in this volume). In this case, a greater number of clouds closer to the center are contributing to the spectra of Seyfert 1 and QSOs, leading to higher $F_{\rm H}$ for these objects as inferred from the models. In addition, since LINERs are low-luminosity objects, we expect lower $F_{\rm H}$ values as shown in Fig. 3.

https://doi.org/10.1017/S0252921100040501 Published online by Cambridge University Press

Regarding the cloud velocity, again assuming the unified model is valid, the velocity for Seyfert 1 and QSOs should, on average, be higher than for Seyfert 2. The velocity in LINERs is expected to be lower on average since they are low-luminosity nuclei and some observational features are characteristic of SD clouds.

The average dust-to-gas ratio for Seyfert 1 and Seyfert 2 are similar, while it is lower for LINERs as expected from the observations.

The non-Gaussian emission-line profiles are another important characteristic of the NLR spectra (Carleton & Vrtilek 1985, Whittle 1985, Buczko & Steiner 1990). Assuming a power-law distribution for the cloud velocities, the composite models offer a large collection of kinematic line profiles to fit to the observations (Contini & Viegas-Aldrovandi 1989). In fact, because the contributions coming from shocks and from photoionization are different for different sets of shock velocity and ionizing radiation intensity, depending on the dust location (inside or outside the emitting clouds), the red side (or the blue side) of the line is fainter, producing an asymmetric profile.

3.3. A Model for NGC 5252

The S0 galaxy NGC 5252, at a redshift of $z \approx 0.023$, shows one of the best examples of anisotropic nuclear radiation, and may be a good example of the AGN unified model. It shows a biconical structure of ionized gas extending up to 17 kpc ($H_0 = 100\,\mathrm{km\,s^{-1}\,Mpc^{-1}}$) from the center of the galaxy (Tadhunter & Tsevatanov 1989), and a Sy 2 spectrum. The kinematics of the neutral gas is in remarkable agreement with that of the ionized gas (Prieto & Freudling 1996). A large amount of observational data has been accumulated for the central region of this galaxy (Kotilanen & Prieto 1995, Cappi et al. 1995, Osterbrock & Martel 1993, Acosta-Pulido et al. 1996), from radio to X-rays, providing the basis for a detailed study of the emission processes .

Recently, a self-consistent model has been proposed assuming that, except for the hard X-rays, both the continuum and the emission-line spectra are produced by shocked clouds reached by the central ionizing radiation (Contini et al. 1996). The observed X-ray spectrum shows two components: a hard X-ray component well characterized by a flat power-law ($\alpha \approx -0.4$), which is strongly absorbed for $E < 1\,\mathrm{keV}$, and an excess at lower energies. We assume that the hard component is nuclear and absorbed by the gas along the line of sight, whereas the soft component is produced by the shocked clouds. If we assume an ionizing radiation spectrum which is an extrapolation of the flat X-ray spectrum towards the UV, photoionization models show that this ionizing radiation is neither strong enough nor has the right slope to provide a good fit to the observed emission-line ratios. Therefore, a composite power-law ionizing continuum is adopted, with UV index equal to -1.5 and an X-ray index equal to -0.4. Because the line spectrum shows high-ionization lines ([Ne V], [Fe X]) and a low [O III] line ratio, we expect that high-velocity, shock-dominated clouds are present in the NLR. The infrared spectrum indicates the presence of dust at different temperatures which may be explained by clouds at different velocities.

In order to account for all the observed features, three main types of clouds must be contributing to the spectra:

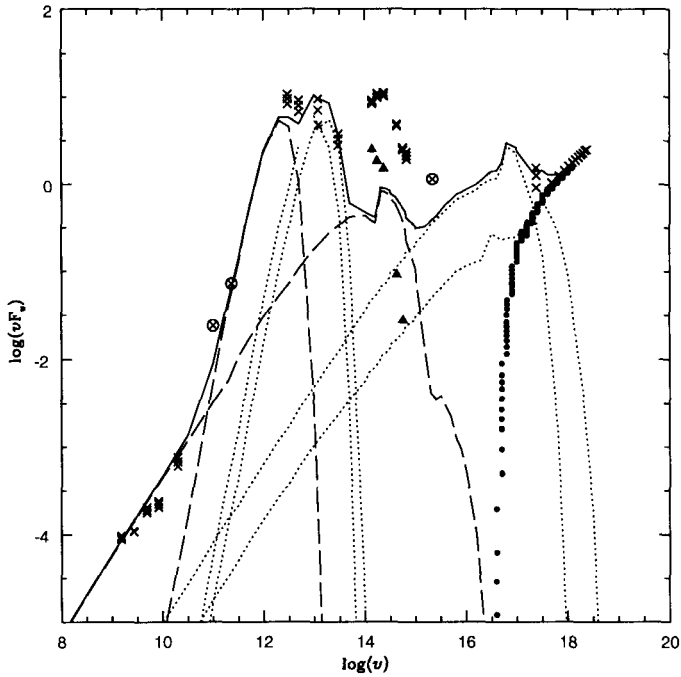

Figure 4. Continuum spectrum of NGC 5252 (νF_ν in units of ergs s^{-1} cm^{-2} and the frequency ν in Hz). See the text for the notation.

- One type of radiation-dominated cloud (RD1) with $v_s = 100\,\mathrm{km\,s^{-1}}$ and $F_\mathrm{H} = 10^9$;
- Two types of shock-dominated clouds, SD1 with $v_s = 400\,\mathrm{km\,s^{-1}}$, and SD2 with $1000\,\mathrm{km\,s^{-1}}$.

The dust-to-gas ratio of the clouds is $1\text{–}2 \times 10^{-14}$. In order to fit all the emission lines as well as the continuum the relative contributions are RD1: SD1: SD2 = 100: 5: 0.02. Most of the lines are produced by the RD1 clouds, however the high-ionization lines come from SD1 and SD2 clouds (Contini et al. 1996). Because of the high velocities, the SD clouds have a high-temperature zone producing strong UV/X-ray diffuse radiation, which in turn results in a wide low-ionization zone producing strong lines too. The fit to the continuum is shown in Fig. 4. The observational data are indicated by crosses, the upper limits by encircled crosses, the stellar-subtracted data by filled triangles. Results for clouds RD1 are indicated by dashed lines, and for SD1 and SD2 by dotted lines. The absorbed nuclear X-ray emission is shown by the filled circles. The solid line is the fit to the continuum, adding up all the contributions according to their weights. The radio and optical continuum is due to RD1 clouds (the

https://doi.org/10.1017/S0252921100040501 Published online by Cambridge University Press

correction of the optical data for stellar emission is very uncertain). The infrared data are fit by dust heated by the central radiation (far IR) and by shocks (near IR). Finally, the soft X-ray excess is due to the high-velocity shocked clouds.

The observed Hα luminosity indicates that the emitting clouds are less than 1 kpc from the center, whereas the observed soft X-ray luminosity implies that the high-velocity clouds are closer (< 30 pc). These results show that composite models can provide a consistent picture of the NLR of NGC 5252.

4. Final Remarks

For many years the presence of shocks in the NLR has been used to solve the problem of an additional energy source. Now images of shocked regions are being seen in AGN, providing direct evidence for this energy source.

Composite models, which incorporate both shocks and photoionization by the central source to determine the physical conditions of the NLR, are seen to be a powerful tool to analyze the NLR. Moreover, they provide a coherent scenario for the NLR. Using these models to fit both the emission-line and continuum spectra of specific objects (as shown for NGC 5252) it is possible to define the 'identity card' of the object, i.e., the dominant velocity of the clouds, their type and location. In particular, since the high-ionization lines, infrared emission and the soft X-ray component should come from high-velocity clouds, the resulting locations offer an observational test to the models through infrared, optical and X-ray imaging.

Notice that the X-ray spectra of a increasing number of AGN show that the contributions of the hard and soft components depend on the type of AGN (Iwasawa et al. 1994, Ptak et al. 1994, Serlemitsos et al. 1996). Usually the hard component is associated with the nuclear source while the soft component is associated with extended hot gas. However, the origin of this thermal component is not well understood. In fact, electron-scattered nuclear flux cannot always explain the soft component because, unless the temperature is less than 10^6 K, the direct contribution from the hot gas would dominate the scattered flux (Elvis et al. 1990). Our composite models provide an alternate origin for this soft component, and its contribution to the X-ray spectra will depend on the type of object. In particular, taking into account the general results summarized in Fig. 3, we expect that the soft component in LINERs is not important, since the NLR clouds must have low velocities, and their X-ray spectra should be dominated by the nuclear emission. This is in perfect agreement with recent observations (Serlemitsos et al. 1996).

Once the main process powering a large sample of NLR is established, the problem of the chemical abundances in AGN can be discussed on a more reliable basis. If photoionization is not the only mechanism acting in these regions, it may be premature to rely on results of standard photoionization models to obtain the chemical composition of the emitting gas. Over-solar or under-solar abundances can only be invoked with confidence if all the physical processes determining physical conditions in the gas are taken into account. Only then, the resulting chemical abundances will provide a reliable tool to probe the chemical evolution of galaxies.

Acknowledgments. S. M. V. is grateful to the Department of Astronomy of the Ohio State University and the Institute for Nuclear Theory at the University of Washington for their hospitality while preparing this paper.

References

Acosta-Pulido, J., Vila-Vilaro, B., Perez, I., Wilson, A. S., & Tsvetanov, Z. 1996, ApJ, 464, 177.

Allen, C. W. 1973, Astrophysical Quantities (London: Athlone Press).

Binette, L., Dopita, M. A., & Tuohy, I. R. 1985, ApJ, 297, 476.

Binette, L., Wilson, A. S., & Storchi-Bergmann, T. 1996, A&A, 312, 365.

Busko, I., & Steiner, J. E. 1990, MNRAS, 245, 470.

Cappi, M., Mihara, T., Matsuoka, M., Brinkmann, W., Prieto, M. A., & Palumbo, G. G., 1995, ApJ, 456, 141.

Carleton, N. P., & Vrtilek, J. M. 1985, ApJ, 294, 106.

Contini, M., & Aldrovandi, S. M. V. 1983, A&A, 127, 15.

Contini, M., & Aldrovandi, S. M. V. 1986, A&A, 168, 41.

Contini, M., Prieto, M. A., & Viegas, S. M. 1996, Proceedings of Science with the Hubble Telescope - II, eds. P. Benvenuti, F. D. Machetto, & E. J. Schreier.

Contini, M., & Viegas-Aldrovandi, S. M. 1989, ApJ, 343, 78.

Cox, D. P. 1972, ApJ, 178, 142.

Elvis, M., Fassnacht, C., Wilson, A. S., & Briel, U. 1990, ApJ, 361, 459.

Ferland, G., & Mushotzky, R. 1984, ApJ, 286, 42.

Filippenko, A. V. 1985, ApJ, 289, 475.

Iwasawa, K., Yaqoob, T., Awaki, H., & Ogasaka, Y. 1994, PASJ, 46, L167.

Koski, A. T. 1978, ApJ, 223, 56.

Kotilanien, J. K., & Prieto, M. A. 1995, A&A, 295, 646.

Malkan, M. A. 1983, ApJ, 268, 582.

Marconi, A., Moorwood, A. F. M., & Oliva, E. 1994, A&A, 291, 18.

Morganti, R., Robinson, A., Fosbury, R. A. E, di Seregho Alighieri, S., Tadhunter, C. N., & Malin, D. F. 1991, MNRAS, 249, 91.

Oliva, E., Salvati, M., Moorwood, A. F. M., & Marconi, A. 1994, A&A, 288, 457.

Osterbrock, D. E. 1983, IAU Symp. 103 on Planetary Nebulae, ed. D. R. Flower (Dordrecht: Reidel), 473.

Osterbrock, D. E. 1989, Astrophysics of Gaseous Nebulae and Active Galactic Nuclei (Mill Valley: University Science Books).

Osterbrock, D. E., & Martel, A. 1993, ApJ, 418, 668.

Parker, R. A. R. 1967, ApJ, 149, 363.

Pogge, R. W. 1997, this volume.

Poveda, A., & Woltjer, L. 1968, AJ, 73, 65.

Prieto, M. A., & Freudling, W. 1996, MNRAS, 279, 63.

Prieto, M.A., Walsh, J., Fosbury, R.A., & di Seregho Alighieri, S. 1993, MNRAS, 263, 10.

Ptak, A., Yaqoob, T., Serlemitsos, P., Mushotzky, R., & Otani, C. 1994, ApJ, 436, L31.

Seyfert, C. 1943, ApJ, 97, 28.

Storchi-Bergmann, T., Wilson, A.S., Mulchaey, J.S., & Binette, L. 1996, A&A, 312, 357.

Sutherland, R.S., Bicknell, G.V., & Dopita, M.A. 1993, ApJ, 414, 510.

Tadhunter, C., & Tsvetanov, Z. 1989, Nature, 341, 42.

Vaceli, M.S., Viegas, S.M., Gruenwald, R., & Benevides-Soares, P. 1993, PASP, 105, 875.

Viegas-Aldrovandi, S.M. 1988, ApJ, 330, L9.

Viegas-Aldrovandi, S.M., & Gruenwald, R.B. 1988, ApJ, 324, 683.

Viegas-Aldrovandi, S.M., & Gruenwald, R.B. 1990, ApJ, 360, 474.

Viegas, S.M., & Contini, M. 1994, ApJ, 408, 113.

Viegas, S.M., & Prieto, M.A. 1992, MNRAS, 258, 483.

Weaver, K., Yaqoob, T., Holt, S., Mushotzky, R., Matsuoka, M., & Yamauchi, M. 1994, 436, L27.

Whittle, M. 1985, MNRAS, 213, 1.

Willner, S.P., Elvis, M., Fabbiano, G., Lawrence, A., & Ward, M.J. 1985, ApJ, 299, 443.

Wilson, A.S., 1997, this volume.